

Cite this: *Chem. Sci.*, 2025, 16, 22465

All publication charges for this article have been paid for by the Royal Society of Chemistry

Received 23rd July 2025  
Accepted 13th October 2025

DOI: 10.1039/d5sc05519a

rsc.li/chemical-science

# The optical response of aromatic cyclocarbons

Simone Grillo,<sup>id</sup>\*<sup>ab</sup> Olivia Pulci<sup>id</sup><sup>a</sup> and Tommaso Giovannini<sup>id</sup>\*<sup>a</sup>

Cyclo[*n*]carbons are a recently synthesized class of carbon allotropes that offer a unique platform to probe electron delocalization, quantum confinement, and strong correlation effects. Their peculiar electronic properties and bond topologies make them attractive for next-generation molecular optoelectronic, photonic, and quantum technologies. To explore such a potential, a deep understanding of their optical response is necessary. Here, we present the first systematic characterization of the optical response of aromatic cyclo[*n*]carbons in the whole UV-Vis range, using state-of-the-art many-body methods. Our results show a remarkable tunability of their optical response with respect to ring size and structure, identifying key structure–property relationships. These findings provide a fundamental framework for tailoring the optical properties of  $\pi$ -conjugated carbon nanorings and offer design principles for their integration into adaptive molecular devices and quantum photonics architectures.

## 1 Introduction

Cyclo[*n*]carbons are planar molecular rings composed exclusively of *n* sp-hybridized carbon atoms.<sup>1</sup> These unusual carbon allotropes have attracted significant interest due to their distinctive structural and electronic properties, making them a fascinating platform for studying electron delocalization, quantum confinement, and strong correlation effects.<sup>2,3</sup> The experimental synthesis of cyclo[18]carbon (C<sub>18</sub>) in the condensed phase in 2019 (ref. 4) marked a pivotal milestone, unveiling its characteristic alternating single-triple bond conjugation pattern.<sup>5</sup> This breakthrough has paved the way for the design and synthesis of additional cyclo[*n*]carbons,<sup>6–9</sup> confirming the stability of these carbon allotropes on surfaces, even for large carbon frameworks.

From early theoretical works to recent on-surface synthesis of larger systems,<sup>4,6–10</sup> these carbon allotropes have transitioned from purely exotic molecules to experimentally accessible systems, enabling systematic studies of their electronic and optical properties. However, despite rapid experimental progress, the fundamental understanding of their optical behavior remains limited, which hampers their potential use as tunable elements in molecular-scale optoelectronics and quantum photonics.<sup>11–16</sup> Theoretical approaches are thus crucial not only to elucidate their intrinsic properties but also to guide technological developments.

In this work, we predict the optical properties of aromatic cyclo[*n*]carbons by using state-of-the-art methods in quantum

chemistry and condensed matter physics, properly describing electron correlation. This is a fundamental prerequisite as their electronic structure is characterized by a  $\pi$ -conjugation pattern,<sup>17</sup> which exhibits complex many-body effects that challenge both conceptual frameworks and computational methods.<sup>6</sup> In particular, our findings identify key trends in the optical response of cyclo[*n*]carbons, clarifying their electronic delocalization, strong electron correlation, and structure–property relationships. Most notably, we demonstrate that the optical gap and spectral features can be finely tuned through structural control by external stimuli. This aspect highlights the versatility of cyclo[*n*]carbons, positioning them as tunable, molecular building blocks for next-generation molecular optoelectronic technologies.

## 2 Results and discussion

We start our analysis with the smallest aromatic cyclo[*n*]carbon exhibiting a polyene electronic structure: C<sub>14</sub> (see Fig. 1a for the CCSD/cc-pVDZ<sup>3</sup> geometrical parameters). To assess the performance of state-of-the-art quantum methods for predicting the optical response of molecular systems,<sup>18,19</sup> the excitation energies are computed using highly correlated wavefunction-based Post-Hartree-Fock (Post-HF) methods (equation of motion coupled cluster EOM-CC2, EOM-CCSD, and EOM-CC3, as well as multireference approaches based on Complete Active Space Second Order Perturbation CASPT2 with 8 electrons in 8 active orbitals), time-dependent density functional theory (TDDFT), and many-body perturbation theory (MBPT) within the Bethe–Salpeter equation (BSE) formalism. It is worth noting that, due to its highly symmetric D<sub>7h</sub> structure, most electronic transitions are dark. As a result, the first bright excitation involves singlet states ranging from S15 to S32, depending on the method. This makes highly correlated excited-state calculations

<sup>a</sup>Department of Physics, University of Rome “Tor Vergata”, INFN, Via della Ricerca Scientifica 1, 00133 Rome, Italy. E-mail: simone.grillo@roma2.infn.it; tommaso.giovannini@uniroma2.it

<sup>b</sup>Max Planck Institute for the Structure and Dynamics of Matter, Luruper Chaussee 149, 22761 Hamburg, Germany



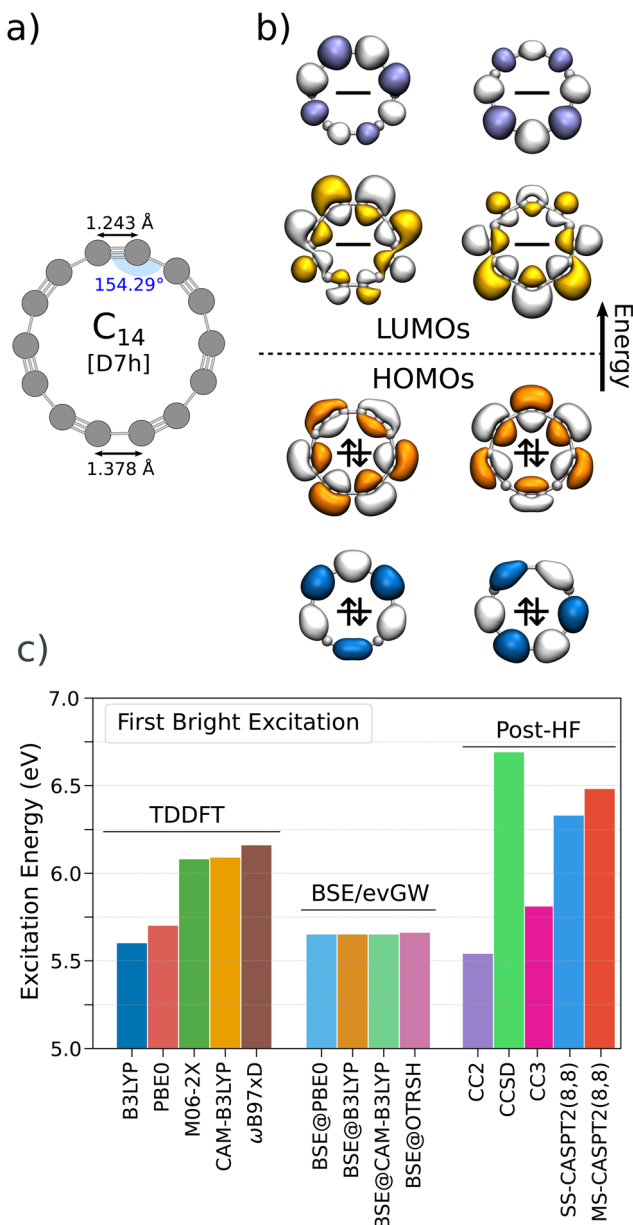


Fig. 1 (a) Molecular structure of  $C_{14}$ . Geometric parameters (bonds and angles) at the CCSD/cc-pVDZ level<sup>3</sup> and point group symmetry are highlighted; (b) graphical depiction of the eight valence MOs involved in the first bright transition of  $C_{14}$ , calculated at the HF/aug-cc-pVDZ level (dark: occupied MOs, light: virtual MOs). (c)  $C_{14}$  excitation energies (eV) of the first bright transition as a function of the level of theory.

particularly demanding, as a large number of singlet states must be converged to fully characterize the optical spectrum in the whole UV-Vis range (see Methods). For this benchmark, we thus focus on the first bright excitation only, which is associated with a  $\pi$ - $\pi^*$  electronic transition (see Fig. 1b). Highly symmetric patterns characterize all involved molecular orbitals (MOs), which are pair-degenerate with the  $\pi$  and  $\pi^*$  MOs displaced in-plane (orange-scale gradient) or out-of-plane (blue-scale gradient). The first excitation involves the eight valence MOs (four highest occupied and four lowest unoccupied MOs)

and occurs between occupied and virtual MOs of the same color scale due to symmetry constraints (see Fig. 1b and S2 in the SI).

In Fig. 1c, the excitation energies of the first bright excitation energy at the considered levels of theory (see also Methods) are graphically depicted (see Table S1 in the SI for raw data). The accuracy of each approach can be judged by comparison with the EOM-CC3 result, which is taken as the reference.<sup>18,19</sup> Among the employed methods, TDDFT is the most computationally affordable, but its performance strongly depends on the exploited exchange-correlation (XC) density functional.<sup>20</sup> Global hybrids such as PBE0 (ref. 21) and B3LYP<sup>22,23</sup> give the closest agreement with CC3, while meta-hybrids (M06-2X<sup>24</sup>) and range-separated hybrids (CAM-B3LYP,<sup>25</sup>  $\omega$ B97xD<sup>26</sup>) progressively deteriorate the accuracy.

To refine the description beyond TDDFT, we turn to the BSE formalism. At this level of theory, quasiparticle energies are first computed by means of the GW approximation and then used to solve the BSE for the excited states. In particular, we employ the eigenvalue self-consistent GW scheme (evGW), which provides reliable quasiparticle energies by self-consistently converging the eigenvalues.<sup>27,28</sup> Remarkably, our results show that the excitation energy is essentially insensitive to the chosen starting functional in the GW calculations (BSE@PBE0, BSE@B3LYP, BSE@CAM-B3LYP, and BSE@optimally tuned range separated hybrid (BSE@OTRSH),<sup>29</sup> see also Methods section). Indeed, the agreement with the reference CC3 calculations is excellent, showing a consistent underestimation of the excitation energy of about 0.15–0.16 eV. EOM-CC2 also performs remarkably well (error 0.27 eV), while EOM-CCSD overestimates the transition energy (0.88 eV). Such a trend has also been reported for other systems, and is generally due to error cancellation at the EOM-CC2 level of theory.<sup>19,30–33</sup> A similar overestimation is also reported at the CASPT2(8,8) level, either by using the state-specific (SS) or multi-state (MS) approach, providing an error of 0.52 eV and 0.67 eV, respectively.

Overall, our results highlight the complex electronic structure of  $C_{14}$ , which requires high-level correlated methods to reproduce the CC3. This is due to the highly delocalized nature of the MOs involved in the transition (see Fig. 1b), which extend over the entire molecular framework, consistent with the conjugated nature of the bonds. Among the tested methods, BSE/evGW and EOM-CC2 provide the best compromise between computational costs and accuracy, with EOM-CC2 also correctly reproducing the reference EOM-CC3 relative intensity of the weak transition at 3 eV (see Fig. S3 in the SI).

We now move to cyclo[18]carbon ( $C_{18}$ ), which is the first experimentally synthesized member of this class,<sup>4</sup> and, also, the most studied cyclo[ $n$ ]carbon from a theoretical point of view.<sup>2,3,12,14,15,34–37</sup> Most of these works focus on the determination of the electronic structure of such a carbon allotrope in the gas phase. However, the successful experimental synthesis of  $C_{18}$  on a NaCl substrate<sup>4</sup> raises the question of whether the substrate influences its electronic structure, and in particular, its optical response. Given the absence of explicit experimental absorption spectra for free-standing  $C_{18}$ , it is crucial to determine whether electrostatic interactions with the underlying



ionic lattice could significantly alter its excitation energies. To this end, we follow the strategy proposed in ref. 6, *i.e.* we employ a multiscale QM/Molecular Mechanics (QM/MM) approach based on electrostatic embedding.<sup>38,39</sup> Within this framework,  $C_{18}$  is treated at the QM level, while the NaCl substrate is described as a fixed array of point charges (+1 and -1), mimicking the ionic nature of the substrate. Such charges enter the QM Hamiltonian *via* the electrostatic interaction with the potential generated by the QM density, which is therefore perturbed and modified by the external field. To minimize boundary effects and ensure a realistic description of the substrate influence, we construct a large NaCl supercell consisting of a  $100 \times 100 \times 100 \text{ \AA}^3$  cubic lattice with a lattice parameter of  $5.44 \text{ \AA}$ .<sup>69</sup> This setup yields a total of 46 656 external point charges and ensures that the electrostatic potential experienced by the  $C_{18}$  is representative of an extended surface (see Fig. 2a and b).

To isolate the purely electrostatic influence of the substrate, the molecular geometry of  $C_{18}$  is not relaxed, and kept fixed at the CCSD/cc-pVDZ geometry recovered from ref. 3. In this way, the direct contribution of the substrate on  $C_{18}$  optical response is dissected from any geometrical effect. This assumption is supported by previous findings reported in ref. 6 and 40, which demonstrate that the presence of NaCl does not introduce any

substantial structural modification on the  $C_{18}$  structure. The molecular system is placed at a distance of  $3.2 \text{ \AA}$  from the NaCl surface, which has been identified as the equilibrium distance in ref. 40 (see Fig. 2a and b). To analyze the dependence of the absorption spectrum on the adsorption site, four adsorption positions are considered by shifting the molecular system by  $1.36 \text{ \AA}$  (lattice constant  $5.44 \text{ \AA}$ ).

To quantitatively assess the impact of the substrate, we compute the absorption spectrum of  $C_{18}$  both *in vacuo* and in the presence of the NaCl substrate (Fig. 2c) at the EOM-CC2/aug-cc-pVDZ level. We exploit EOM-CC2 for the reliability of the reproduction of EOM-CC3 results for  $C_{14}$ , by using the electrostatic QM/MM implementation provided in the electronic structure program eT (see Methods). All four structures are nearly isoenergetic (maximum difference about  $0.2 \text{ kcal mol}^{-1}$ ), indicating that the cyclocarbon can diffuse almost freely on the NaCl surface, in agreement with previous calculations<sup>40</sup> and experimental data.<sup>4</sup> All spectra shown in Fig. 2 are characterized by three main peaks, and are almost superimposed, demonstrating that the substrate and the adsorption site do not affect  $C_{18}$  optical properties (see Table S2 in the SI for the raw data). Notably, this is also valid by using EOM-CCSD, demonstrating that such a result is valid for different levels of theory as well (see Fig. S7 in the SI). The MOs involved in the bright excitations computed at the various levels are shown in Fig. S6 in the SI. As for  $C_{14}$ , the allowed transitions are associated with  $\pi-\pi^*$  electronic transitions, with the first excitation involving the eight frontier MOs (four highest occupied and four lowest unoccupied MOs), and all the remaining MOs involved in the second and third excitations. Remarkably, at the EOM-CC2 level, the first bright excitation presents a shoulder at about  $5.5 \text{ eV}$  (which is hindered under the first band in all other methods, see Fig. S8 in the SI), which is associated to  $\pi-\pi^*$  electronic transitions involving the same MOs depicted in Fig. S6 in the SI.

As stated above, the spectra of  $C_{18}$ , *in vacuo* or adsorbed on NaCl, show minimal differences, with the spectral features remaining essentially unchanged and with only negligible shifts observed. However, the convoluted spectrum of  $C_{18}$  on NaCl hides a richer underlying structure, arising from the activation of multiple electronic excitations that are optically forbidden in the gas phase, due to the symmetry breaking induced by the external potential of the surface (see Fig. S7 in the SI). Nevertheless, our findings strongly suggest that the electrostatic environment provided by an inert substrate such as NaCl<sup>4</sup> should not significantly perturb the optical response of  $C_{18}$ .

This result reinforces our benchmark calculations on  $C_{14}$  in gas-phase and allows us to perform all the following calculations *in vacuo*, remarking, however, that a different substrate can potentially tune the optical response. This indeed raises the question of under what conditions the optical response of cyclocarbons can be modulated in the pursuit of optoelectronics. One of the most exploited mechanisms in molecular optoelectronics is the tunability of the optical response as a function of the equilibrium geometry,<sup>41-43</sup> which can be altered by external stimuli – for instance, mechanical strain or pressure, external electric field, or chemical functionalization by means of controlled interaction with substrates.



Fig. 2 (a and b) Graphical depiction of  $C_{18}$  in the gas-phase (a) and adsorbed on a NaCl surface at four different positions (b). Geometric parameters (bonds and angles) at the CCSD/cc-pVDZ level<sup>3</sup> and point group symmetry are highlighted; (c) EOM-CC2/aug-cc-pVDZ optical spectra of  $C_{18}$  *in vacuo* (dashed blue) and adsorbed on NaCl at four different positions. A Gaussian-type broadening (FWHM =  $0.3 \text{ eV}$ ) is used.



In our analysis, we adopt the CCSD/cc-pVDZ geometry from ref. 3, as it correctly predicts the experimental polyne structure.<sup>4</sup> However, the theoretically optimized geometry of  $C_{18}$  varies across diverse computational studies depending on the electronic structure methodology exploited for structure determination, yielding different bond lengths and bond length alternation (BLA) patterns, underscoring the sensitivity of the system to electronic correlation and exchange effects.<sup>3,4,15,17,40,44</sup>

To simulate the effect of an external stimulus, we therefore compare two  $C_{18}$  geometries, optimized at different levels of theory. In particular, we consider the CCSD/cc-pVDZ reference geometry and an alternative structure optimized at the DFT level using plane waves (PWs), employing a HSE XC functional,<sup>45</sup> where the HF exchange is increased to 80%. In this way, the obtained geometric parameters are in excellent agreement with previously reported values in the literature.<sup>4,15</sup> Both structures exhibit a  $D_{9h}$  symmetry polyne-like arrangement, yet display slight differences in their triple and single bond lengths, which in the HSE geometry decrease by 0.033 Å and 0.024 Å, respectively, when compared to CCSD/cc-pVDZ (see Fig. 3a). Consequently, the BLA parameter increases from 0.145 Å (CCSD/cc-pVDZ) to 0.154 Å (HSE).

To evaluate the impact of the structural variations on the optical response, we compute the excitation energies using the

electronic structure methods previously employed for the analysis of  $C_{18}$  response. The results obtained at the EOM-CC2/aug-cc-pVDZ level are reported in Fig. 3b. The spectra computed using all other methods are also given in Fig. S9 in the SI. Remarkably, despite the minimal geometric differences on the order of tens of mÅ, we observe a relative shift of approximately 0.26–0.33 eV in the absorption spectrum, while the overall spectral profile remains unchanged. Such an outcome is similarly observed in all theoretical electronic structure methods (see Fig. S9 and Table S3 in the SI). These findings are particularly surprising and suggest a potential technological advantage for this class of systems: even subtle mechanical distortions could fine-tune the optical absorption of  $C_{18}$  over a significant energy range. These results open opportunities for cyclo[ $n$ ]carbon-based adaptive materials, where geometric modulation could serve as an efficient strategy for optical property control in next-generation molecular photonics and tunable nanoscale devices. Also, they advocate for a proper, reliable, and possibly direct experimental validation of the theoretical structures, for instance, through high-resolution spectroscopic techniques such as rotational, vibrational, or Raman spectroscopy, which could provide precise structural parameters.

The other intuitive method to tune the optical response of cyclocarbons is to vary their size. To this end, we extend our analysis to the optical properties of three additional aromatic cyclo[ $n$ ]carbons, namely  $C_{14}$ ,  $C_{22}$  and  $C_{26}$ . To ensure consistency, all geometries are optimized at the CCSD/cc-pVDZ level ( $C_{14}$  and  $C_{22}$  are recovered from ref. 3), and display a polyne-like bond alternation pattern with  $D_{7h}$  ( $C_{14}$ ),  $D_{11h}$  ( $C_{22}$ ) and  $D_{13h}$  ( $C_{26}$ , see Methods) symmetry (see also Fig. 4a). The BLA index increases by increasing the ring size, moving from 0.135 Å ( $C_{14}$ ) to 0.148 Å ( $C_{22}$ ) and to 0.149 Å ( $C_{26}$ ). As for  $C_{18}$ , the absorption spectra are computed using all the selected electronic structure methods (see Methods section). The computed results are reported in Fig. S1 ( $C_{14}$ ), S4 ( $C_{18}$ ), S11 ( $C_{22}$ ) and S14 ( $C_{26}$ ) in the SI (raw data in Table S1, S2, S4 and S5 in the SI, respectively), and confirm the trends discussed for  $C_{18}$ . It is also worth noting that, although the huge computational cost associated with the theoretical methods, especially EOM-CC2 and EOM-CCSD, we characterize the optical spectrum of the selected aromatic cyclocarbons in the whole UV-Vis range (from 3 to 8 eV), going beyond the calculation of the first bright excitation as previously reported for  $C_{18}$  only.<sup>35,46</sup>

The absorption spectra of all the studied carbon allotropes exhibit three dominant bright excitations involving MOs with a similar nature (see Fig. S2, S6, S12 and S15 in the SI). These findings demonstrate that, despite variations in ring size, all aromatic cyclo[ $n$ ]carbons share a common electronic structure, where strong electron correlation and delocalization effects dictate the optical response. As stated above, for the smallest carbon ring ( $C_{14}$ ), a weak transition appears at around 3 eV (see Fig. S3 in the SI). Such transition is also predicted for  $C_{18}$  (Fig. S10 in the SI),  $C_{22}$  (Fig. S13 in the SI), and  $C_{26}$  (Fig. S16 in the SI), but its intensity decreases as the ring size increases, becoming almost dark for the largest rings ( $C_{18}$ ,  $C_{22}$  and  $C_{26}$ ).



Fig. 3 (a) Graphical depiction of  $C_{18}$  molecular geometry as optimized at the CCSD/cc-pVDZ<sup>3</sup> (Geom. CCSD, left) and at the HSE (80% HF exchange)/plane wave (Geom. HSE, right) levels. (b) EOM-CC2/aug-cc-pVDZ optical spectra of  $C_{18}$  as a function of the molecular structure (blue: Geom. CCSD; red: Geom. HSE). A Gaussian-type broadening (FWHM = 0.3 eV) is used.



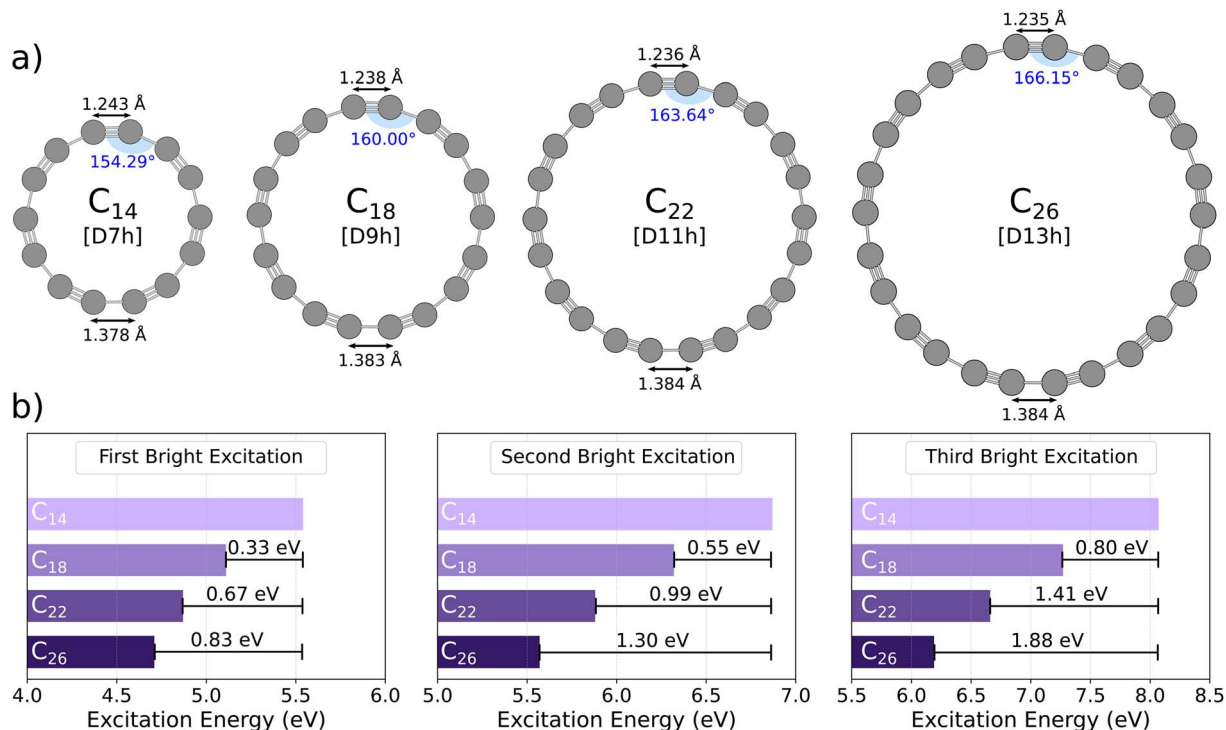


Fig. 4 (a) Molecular geometries of the studied cyclo[n]carbons. Geometric parameters (bonds and angles) at the CCSD/cc-pVDZ level (C<sub>14</sub>–C<sub>22</sub>, from ref. 3) and point group symmetry are highlighted. (b) C<sub>14</sub> (light), C<sub>18</sub> (medium-light), C<sub>22</sub> (medium-dark), and C<sub>26</sub> (dark) excitation energies of the first, second, and third bright transitions calculated at the EOM-CC2/aug-cc-pVDZ level. The energy shifts are also reported.

The evolution of the first bright excitation energy as a function of ring size is systematically analyzed in Fig. 4b at the EOM-CC2/aug-cc-pVDZ level (see also Fig. S17–S19 and Table S6 in SI for the results obtained at the other levels of theory). A decrease of the excitation energies by increasing the ring size is predicted by all approaches, consistently with the expected behavior for quantum confinement in a delocalized  $\pi$ -system, where increasing system size reduces the energy gap between frontier molecular orbitals.<sup>47</sup> The energy shifts by enlarging the ring size depend on the electronic transitions: for the first two bright excitations, they range from 0.33 eV (C<sub>14</sub>–C<sub>18</sub>) to 0.67 eV (C<sub>14</sub>–C<sub>22</sub>) and 0.83 eV (C<sub>14</sub>–C<sub>26</sub>). The third excitation displays the largest energy shift that almost reaches 2 eV when moving from C<sub>14</sub> to C<sub>26</sub> (1.88 eV). Similar trends are also obtained by all other methods (see Fig. S17–S19 and Table S6 in SI). Remarkably, these results suggest that, beyond external perturbations such as mechanical strain or electrostatic fields, controlled modifications of ring size could serve as a powerful and predictable strategy for engineering the optical properties of cyclo[n]carbons.

### 3 Conclusions

In this work, we have presented a theoretical investigation of the optical response of aromatic cyclo[n]carbons, focusing on how their spectroscopic features can be modulated through structural and environmental control. Our results first reveal that carbon nanorings share a common optical fingerprint consisting of three dominant bright  $\pi$ - $\pi^*$  transitions, whose excitation energies decrease systematically with increasing ring size,

spanning more than 1 eV between C<sub>14</sub> and C<sub>26</sub>. This trend reflects the delocalized nature of their  $\pi$ -electron systems and establishes the ring size as an effective handle for tuning their optoelectronic properties.

By analyzing the case of C<sub>18</sub> in the presence of an electrostatic embedding model for the NaCl substrate, we also demonstrate that an inert ionic environment used in experimental synthesis does not significantly perturb the absorption spectrum. However, our calculations show that even subtle changes in the molecular geometry, such as small variations in single and triple bond lengths, can induce spectral shifts on the order of 0.2–0.3 eV. This remarkable sensitivity highlights the potential for finely controlling the optical properties of cyclo[n]carbons through external stimuli, such as mechanical strain, electric fields, or chemical functionalization.

To conclude, our findings demonstrate that the optical response of cyclo[n]carbons can be engineered through both intrinsic (geometry, ring size) and extrinsic (substrate, environment) parameters, making them promising candidates for applications in nanoscale optoelectronics, photonics, and quantum technologies. This study establishes a rigorous theoretical foundation that can guide future experimental efforts and support the design of functional carbon-based molecular devices.

### 4 Methods

Cyclo[n]carbons ( $n = 14, 18, 22$ ) geometries are recovered from ref. 3, and are optimized at the CCSD/cc-pVDZ level of theory. C<sub>18</sub> geometry is also optimized using a plane wave (PW)-based



method within the framework of DFT, as implemented in the Quantum ESPRESSO package.<sup>48,49</sup> The range-separated hybrid functional HSE<sup>45</sup> with an increased HF exchange (80%) is used, following previous studies.<sup>4,15</sup> The geometry of cyclo[26]carbon is extrapolated from smaller members of the series and verified at the CCSD/cc-pVDZ level, confirming that it corresponds to a local minimum (Root Mean Square force smaller than  $3 \times 10^{-4}$  a.u.). The optical properties of the selected cyclo[*n*]carbons are computed by using various electronic structure methods. In all cases, the aug-cc-pVDZ basis set is exploited. For the specific case of cyclo[18]carbon, the spectra are also calculated using the aug-cc-pVTZ basis set (see Fig. S5 in the SI), showing an almost perfect superposition with the aug-cc-pVDZ counterparts (see also Table S2 in the SI for raw data), thus demonstrating basis-set convergence. TDDFT calculations using global-hybrids (B3LYP, PBE0), *meta*-GGA hybrid (M06-2X), and range-separated hybrid (CAM-B3LYP,  $\omega$ B97xD) density functionals are performed by using PySCF.<sup>50,51</sup> All calculations are performed by requesting 100 excitations. Equation-of-motion (EOM)-CC2, EOM-CCSD, and multiscale EOM-CCSD/MM calculations are also performed using the electronic structure code eT.<sup>52</sup> For EOM-CC2, 100 excitations are required, while for EOM-CCSD equations are solved for 100 states ( $C_{14}$ ), 80 states ( $C_{18}$ ,  $C_{22}$ ), and 70 states ( $C_{26}$ ). EOM-CC3 calculations on  $C_{14}$  are performed by requiring 32 excited states. BSE/evGW calculations are performed by exploiting the resolution-of-identity approximation as implemented in the molGW code,<sup>53</sup> requesting in all cases 100 excitations. GW corrections are applied to a ground state computed at the B3LYP, PBE0, CAM-B3LYP, and optimally-tuned range-separated hybrid (OTRSH) levels. The OTRSH  $\gamma$  parameter is optimized for each cyclo[*n*]carbon as proposed in ref. 29 by enforcing the DFT ionization potential theorem (using the cationic expression only).<sup>54,55</sup> The resulting  $\gamma$  parameters are: 0.2 ( $C_{14}$ ), 0.17 ( $C_{18}$ ), 0.18 ( $C_{22}$ ), 0.16 ( $C_{26}$ ). SS- and MS-CASPT2(8,8) calculations are performed by using OpenMolcas.<sup>56</sup> CASPT2 wavefunction is constructed on top of a state-average CASSCF calculation by using 8 active electrons in 8 active MOs, that are represented in Fig. 1b ( $C_{14}$ ), S6 in the SI ( $C_{18}$ ), S12 in the SI ( $C_{22}$ ), and S15 in the SI ( $C_{26}$ ). The aug-cc-pVDZ basis set is expanded (through the EXPBAS procedure) by starting from an ANO-RCC-MB basis set. 25 states are requested for all CASPT2 calculations.

## Author contributions

S. G. and T. G. performed all calculations. All the authors analyzed and discussed the results. O. P. and T. G. supervised the work. All authors contributed to the writing of the manuscript.

## Conflicts of interest

There are no conflicts to declare.

## Data availability

The data that support the findings of this study are also available from the corresponding author upon request.

Supplementary information is available. See DOI: <https://doi.org/10.1039/d5sc05519a>.

## Acknowledgements

S. G. and O. P. acknowledge PRIN2020 PHOTO, CN1 Spoke6, and INFN project TIME2QUEST. S. G. acknowledges Mariella Ippolito and Fabien Bruneval, and T. G. acknowledges Chiara Cappelli. Computing facilities provided by CINECA HPC center (Iskra C project "CYCLOPS") are also acknowledged.

## References

- H. L. Anderson, C. W. Patrick, L. M. Scriven and S. L. Woltering, A short history of cyclocarbons, *Bull. Chem. Soc. Jpn.*, 2021, **94**, 798–811.
- F. Diederich, Y. Rubin, C. B. Knobler, R. L. Whetten, K. E. Schriver, K. N. Houk and Y. Li, All-carbon molecules: evidence for the generation of cyclo [18] carbon from a stable organic precursor, *Science*, 1989, **245**, 1088–1090.
- S. Arulmozhiraja and T. Ohno, CCSD calculations on  $C_{14}$ ,  $C_{18}$ , and  $C_{22}$  carbon clusters, *J. Chem. Phys.*, 2008, **128**, 114301.
- K. Kaiser, L. M. Scriven, F. Schulz, P. Gawel, L. Gross and H. L. Anderson, An sp-hybridized molecular carbon allotrope, cyclo [18] carbon, *Science*, 2019, **365**, 1299–1301.
- L. Gross, B. Schuler, N. Pavliček, S. Fatayer, Z. Majzik, N. Moll, D. Peña and G. Meyer, Atomic force microscopy for molecular structure elucidation, *Angew. Chem., Int. Ed.*, 2018, **57**, 3888–3908.
- F. Albrecht, I. Rončević, Y. Gao, F. Paschke, A. Baiardi, I. Tavernelli, S. Mishra, H. L. Anderson and L. Gross, The odd-number cyclo [13] carbon and its dimer, cyclo [26] carbon, *Science*, 2024, **384**, 677–682.
- L. Sun, W. Zheng, F. Kang, W. Gao, T. Wang, G. Gao and W. Xu, On-surface synthesis and characterization of anti-aromatic cyclo [12] carbon and cyclo [20] carbon, *Nat. Commun.*, 2024, **15**, 7649.
- L. Sun, W. Zheng, W. Gao, F. Kang, M. Zhao and W. Xu, On-surface synthesis of aromatic cyclo [10] carbon and cyclo [14] carbon, *Nature*, 2023, **623**, 972–976.
- Y. Gao, F. Albrecht, I. Rončević, I. Etedgui, P. Kumar, L. M. Scriven, K. E. Christensen, S. Mishra, L. Righetti, M. Rossmannek, I. Tavernelli, H. L. Anderson and L. Gross, On-surface synthesis of a doubly anti-aromatic carbon allotrope, *Nature*, 2023, **623**, 977–981.
- Y. Gao, P. Gupta, I. Rončević, C. Mycroft, P. J. Gates, A. W. Parker and H. L. Anderson, Solution-phase stabilization of a cyclocarbon by catenane formation, *Science*, 2025, **389**, 708–710.
- R. Ng, M. Portnoi and R. Hartmann, Tuning terahertz transitions in cyclo [*n*] carbon rings, *Phys. Rev. B*, 2022, **106**, L041403.
- S. Fang and Y. H. Hu, Cyclo [18] carbon as an ultra-elastic molecular O-ring with unique mechanical properties, *Carbon*, 2021, **171**, 96–103.



- 13 L. Zhang, H. Li, Y. P. Feng and L. Shen, Diverse transport behaviors in cyclo [18] carbon-based molecular devices, *J. Phys. Chem. Lett.*, 2020, **11**, 2611–2617.
- 14 Z. Liu, T. Lu and Q. Chen, Intermolecular interaction characteristics of the all-carboatomic ring, cyclo [18] carbon: Focusing on molecular adsorption and stacking, *Carbon*, 2021, **171**, 514–523.
- 15 Z. S. Pereira and E. Z. da Silva, Spontaneous symmetry breaking in cyclo [18] carbon, *J. Phys. Chem. A*, 2020, **124**, 1152–1157.
- 16 M. M. Haley, Cyclo [18] carbon, the newest member of the family of carbon allotropes, *Chem*, 2019, **5**, 2517–2519.
- 17 Pooja, S. Yadav and R. Pawar, Chemistry of Cyclo [18] Carbon (C18): A Review, *Chem. Rec.*, 2024, **24**, e202400055.
- 18 P.-F. Loos, M. Boggio-Pasqua, A. Blondel, F. Lipparini and D. Jacquemin, QUEST Database of Highly-Accurate Excitation Energies, *J. Chem. Theory Comput.*, 2025, **21**, 8010–8033.
- 19 I. Knysh, F. Lipparini, A. Blondel, I. Duchemin, X. Blase, P.-F. Loos and D. Jacquemin, Reference CC3 excitation energies for organic chromophores: Benchmarking TD-DFT, BSE/GW, and wave function methods, *J. Chem. Theory Comput.*, 2024, **20**, 8152–8174.
- 20 C. Adamo and D. Jacquemin, The calculations of excited-state properties with Time-Dependent Density Functional Theory, *Chem. Soc. Rev.*, 2013, **42**, 845–856.
- 21 C. Adamo and V. Barone, Toward reliable density functional methods without adjustable parameters: The PBE0 model, *J. Chem. Phys.*, 1999, **110**, 6158–6170.
- 22 A. D. Becke, Density-functional thermochemistry. III. The role of exact exchange, *J. Chem. Phys.*, 1993, **98**, 5648–5652.
- 23 P. Stephens, F. Devlin, C. Chabalowski and M. J. Frisch, Ab initio calculation of vibrational absorption and circular dichroism spectra using density functional force fields, *J. Phys. Chem.*, 1994, **98**, 11623–11627.
- 24 Y. Zhao and D. G. Truhlar, The M06 suite of density functionals for main group thermochemistry, thermochemical kinetics, noncovalent interactions, excited states, and transition elements: two new functionals and systematic testing of four M06-class functionals and 12 other functionals, *Theor. Chem. Acc.*, 2008, **120**, 215–241.
- 25 T. Yanai, D. P. Tew and N. C. Handy, A new hybrid exchange–correlation functional using the Coulomb-attenuating method (CAM-B3LYP), *Chem. Phys. Lett.*, 2004, **393**, 51–57.
- 26 J.-D. Chai and M. Head-Gordon, Long-range corrected hybrid density functionals with damped atom–atom dispersion corrections, *Phys. Chem. Chem. Phys.*, 2008, **10**, 6615–6620.
- 27 D. Jacquemin, I. Duchemin, A. Blondel and X. Blase, Assessment of the accuracy of the Bethe–Salpeter (BSE/GW) oscillator strengths, *J. Chem. Theory Comput.*, 2016, **12**, 3969–3981.
- 28 D. Jacquemin, I. Duchemin and X. Blase, Is the Bethe–Salpeter formalism accurate for excitation energies? Comparisons with TD-DFT, CASPT2, and EOM-CCSD, *J. Phys. Chem. Lett.*, 2017, **8**, 1524–1529.
- 29 C. A. McKeon, S. M. Hamed, F. Bruneval and J. B. Neaton, An optimally tuned range-separated hybrid starting point for *ab initio* GW plus Bethe–Salpeter equation calculations of molecules, *J. Chem. Phys.*, 2022, **157**, 074103.
- 30 P.-F. Loos and D. Jacquemin, A mountaineering strategy to excited states: Highly accurate energies and benchmarks for bicyclic systems, *J. Phys. Chem. A*, 2021, **125**, 10174–10188.
- 31 M. V eril, A. Scemama, M. Caffarel, F. Lipparini, M. Boggio-Pasqua, D. Jacquemin and P.-F. Loos, QUESTDB: A database of highly accurate excitation energies for the electronic structure community, *WIREs: Comput. Mol. Sci.*, 2021, **11**, e1517.
- 32 M. Schreiber, M. R. Silva-Junior, S. Sauer and W. Thiel, Benchmarks for electronically excited states: CASPT2, CC2, CCSD, and CC3, *J. Chem. Phys.*, 2008, **128**, 134110.
- 33 D. K ann ar and P. G. Szalay, Benchmarking coupled cluster methods on valence singlet excited states, *J. Chem. Theory Comput.*, 2014, **10**, 3757–3765.
- 34 D. A. Plattner and K. Houk, C18 is a polyyne, *J. Am. Chem. Soc.*, 1995, **117**, 4405–4406.
- 35 Z. Liu, T. Lu and Q. Chen, An sp-hybridized all-carboatomic ring, cyclo [18] carbon: Electronic structure, electronic spectrum, and optical nonlinearity, *Carbon*, 2020, **165**, 461–467.
- 36 G. V. Baryshnikov, R. R. Valiev, L. I. Valiulina, A. E. Kurtsevich, T. Kurt en, D. Sundholm, M. Pittelkow, J. Zhang and H.  gren, Odd-number cyclo [n] carbons sustaining alternating aromaticity, *J. Phys. Chem. A*, 2022, **126**, 2445–2452.
- 37 G. V. Baryshnikov, R. R. Valiev, R. T. Nasibullin, D. Sundholm, T. Kurten and H.  gren, Aromaticity of even-number cyclo [n] carbons (n= 6–100), *J. Phys. Chem. A*, 2020, **124**, 10849–10855.
- 38 A. Warshel and M. Levitt, Theoretical studies of enzymic reactions: dielectric, electrostatic and steric stabilization of the carbonium ion in the reaction of lysozyme, *J. Mol. Biol.*, 1976, **103**, 227–249.
- 39 H. M. Senn and W. Thiel, QM/MM methods for biomolecular systems, *Angew. Chem., Int. Ed.*, 2009, **48**, 1198–1229.
- 40 G. V. Baryshnikov, R. R. Valiev, A. V. Kuklin, D. Sundholm and H.  gren, Cyclo [18] carbon: Insight into electronic structure, aromaticity, and surface coupling, *J. Phys. Chem. Lett.*, 2019, **10**, 6701–6705.
- 41 D. Kos, D. R. Assumpcao, C. Guo and J. J. Baumberg, Quantum tunneling induced optical rectification and plasmon-enhanced photocurrent in nanocavity molecular junctions, *ACS Nano*, 2021, **15**, 14535–14543.
- 42 G. Dushaq, S. Serunjogi, S. R. Tamalampudi and M. Rasras, Electro-optic tuning in composite silicon photonics based on ferroionic 2D materials, *Light: Sci. Appl.*, 2024, **13**, 92.
- 43 Q. Li and Z. Li, Molecular packing: another key point for the performance of organic and polymeric optoelectronic materials, *Acc. Chem. Res.*, 2020, **53**, 962–973.
- 44 Z. Liu, T. Lu and Q. Chen, An sp-hybridized all-carboatomic ring, cyclo [18] carbon: Bonding character, electron delocalization, and aromaticity, *Carbon*, 2020, **165**, 468–475.



- 45 J. Heyd, G. E. Scuseria and M. Ernzerhof, Hybrid functionals based on a screened Coulomb potential, *J. Chem. Phys.*, 2003, **118**, 8207–8215.
- 46 B. Shi, L. Yuan, T. Tang, Y. Yuan and Y. Tang, Study on electronic structure and excitation characteristics of cyclo [18] carbon, *Chem. Phys. Lett.*, 2020, **741**, 136975.
- 47 M. Li, Z. Gao, Y. Han, Y. Zhao, K. Yuan, S. Nagase, M. Ehara and X. Zhao, Potential molecular semiconductor devices: cyclo-C<sub>n</sub> (n= 10 and 14) with higher stabilities and aromaticities than acknowledged cyclo-C<sub>18</sub>, *Phys. Chem. Chem. Phys.*, 2020, **22**, 4823–4831.
- 48 P. Giannozzi, S. Baroni, N. Bonini, M. Calandra, R. Car, C. Cavazzoni, D. Ceresoli, G. L. Chiarotti, M. Cococcioni, I. Dabo, A. Dal Corso, S. de Gironcoli, S. Fabris, G. Fratesi, R. Gebauer, U. Gerstmann, C. Gougoussis, A. Kokalj, M. Lazzeri, L. Martin-Samos, N. Marzari, F. Mauri, R. Mazzarello, S. Paolini, A. Pasquarello, L. Paulatto, C. Sbraccia, S. Scandolo, G. Sclauzero, A. P. Seitsonen, A. Smogunov, P. Umari and R. M. Wentzcovitch, QUANTUM ESPRESSO: a modular and open-source software project for quantum simulations of materials, *J. Phys. Condens. Matter*, 2009, **21**, 395502.
- 49 P. Giannozzi, S. Baroni, N. Bonini, M. Calandra, R. Car, C. Cavazzoni, D. Ceresoli, G. L. Chiarotti, M. Cococcioni, I. Dabo, A. Dal Corso, S. de Gironcoli, S. Fabris, G. Fratesi, R. Gebauer, U. Gerstmann, C. Gougoussis, A. Kokalj, M. Lazzeri, L. Martin-Samos, N. Marzari, F. Mauri, R. Mazzarello, S. Paolini, A. Pasquarello, L. Paulatto, C. Sbraccia, S. Scandolo, G. Sclauzero, A. P. Seitsonen, A. Smogunov, P. Umari and R. M. Wentzcovitch, Advanced capabilities for materials modelling with Quantum ESPRESSO, *J. Phys. Condens. Matter*, 2017, **29**, 465901.
- 50 Q. Sun, T. C. Berkelbach, N. S. Blunt, G. H. Booth, S. Guo, Z. Li, J. Liu, J. D. McClain, E. R. Sayfutyarova, S. Sharma, S. Wouters and G. K.-L. Chan, PySCF: the Python-based simulations of chemistry framework, *Wiley Interdiscip. Rev.: Comput. Mol. Sci.*, 2018, **8**, e1340.
- 51 Q. Sun, X. Zhang, S. Banerjee, P. Bao, M. Barbry, N. S. Blunt, N. A. Bogdanov, G. H. Booth, J. Chen, Z.-H. Cui, J. J. Eriksen, Y. Gao, S. Guo, J. Hermann, M. R. Hermes, K. Koh, P. Koval, S. Lehtola, Z. Li, J. Liu, N. Mardirossian, J. D. McClain, M. Motta, B. Mussard, H. Q. Pham, A. Pulkin, W. Purwanto, P. J. Robinson, E. Ronca, E. R. Sayfutyarova, M. Scheurer, H. F. Schurkus, J. E. T. Smith, C. Sun, S.-N. Sun, S. Upadhyay, L. K. Wagner, X. Wang, A. White, J. D. Whitfield, M. J. Williamson, S. Wouters, J. Yang, J. M. Yu, T. Zhu, T. C. Berkelbach, S. Sharma, A. Y. Sokolov and G. K.-L. Chan, Recent developments in the PySCF program package, *J. Chem. Phys.*, 2020, **153**, 024109.
- 52 S. D. Folkestad, E. F. Kjonstad, R. H. Myhre, J. H. Andersen, A. Balbi, S. Coriani, T. Giovannini, L. Goletto, T. S. Haugland, A. Hutcheson, I.-M. Hoyvik, T. Moitra, A. C. Paul, M. Scavino, A. S. Skeidsvoll, A. H. Tveten and H. Koch, eT 1.0: An open source electronic structure program with emphasis on coupled cluster and multilevel methods, *J. Chem. Phys.*, 2020, **152**, 184103.
- 53 F. Bruneval, T. Rangel, S. M. Hamed, M. Shao, C. Yang and J. B. Neaton, molgw 1: Many-body perturbation theory software for atoms, molecules, and clusters, *Comput. Phys. Commun.*, 2016, **208**, 149–161.
- 54 J. P. Perdew, R. G. Parr, M. Levy and J. L. Balduz Jr, Density-functional theory for fractional particle number: derivative discontinuities of the energy, *Phys. Rev. Lett.*, 1982, **49**, 1691.
- 55 U. Salzner and R. Baer, Koopmans' springs to life, *J. Chem. Phys.*, 2009, **131**, 231101.
- 56 I. F. Galvan, M. Vacher, A. Alavi, C. Angeli, F. Aquilante, J. Autschbach, J. J. Bao, S. I. Bokarev, N. A. Bogdanov, R. K. Carlson, L. F. Chibotaru, J. Creutzberg, N. Dattani, M. G. Delcey, S. S. Dong, A. Dreuw, L. Freitag, L. M. Frutos, L. Gagliardi, F. Gendron, A. Giussani, L. Gonzalez, G. Grell, M. Guo, C. E. Hoyer, M. Johansson, S. Keller, S. Knecht, G. Kovacevic, E. Kallman, G. Li Manni, M. Lundberg, Y. Ma, S. Mai, J. P. Malhado, P. A. Malmqvist, P. Marquetand, S. A. Mewes, J. Norell, M. Olivucci, M. Oppel, Q. M. Phung, K. Pierloot, F. Plasser, M. Reiher, A. M. Sand, I. Schapiro, P. Sharma, C. J. Stein, L. K. Sorensen, D. G. Truhlar, M. Ugandi, L. Ungur, A. Valentini, S. Vancoillie, V. Veryazov, O. Weser, T. A. Wesolowski, P.-O. Widmark, S. Wouters, A. Zech, J. P. Zobel and R. Lindh, OpenMolcas: From Source Code to Insight, *J. Chem. Theory Comput.*, 2019, **15**, 5925–5964.

